Available online at www.sciencedirect.com
ScienceDirect
Journal of Nuclear Materials 359 (2006) 174–184
journal of nuclear materials
www.elsevier.com/locate/jnucmat

Simulations of heat and oxygen diffusion in UO_2 nuclear fuel rods

J.C. Ramirez *, M. Stan, P. Cristea

Los Alamos National Laboratory, P.O. Box 1663, MS G755, Los Alamos, NM 87544, USA

Received 15 May 2006; accepted 18 August 2006

Abstract

We present finite-element simulations of coupled heat and oxygen atom diffusion for UO_2 fuel pellets. The expressions for thermal conductivity, specific heat and oxygen diffusivity for the fuel element are obtained directly from previously published correlations, or from analysis of previously published data. We examine the temperature and non-stoichiometry distributions for a varying range of conditions. Simulations are performed for steady-state and transient regime in one-dimensional (purely radial) configurations. For steady-state conditions we perform parametric studies that determine the maximum temperature in the fuel rod as a function of non-stoichiometry and heat generation rate intensity. For transient simulations, we examine the time lag in the response of the temperature and non-stoichiometry distributions with respect to sudden changes in heat generation rate intensity and oxygen removal rate. All simulations are performed with the commercial code COMSOL Multiphysics™.

PACS: 28.41.Ak; 44.10.+i; 66.10.Cb

1. Introduction

Mixed oxide fuels (of which UO_2 can be considered a special case) are very popular choices for light water reactors and have been recently considered as fuel for fast breeder reactors [1]. A review of fuel performance codes [2] shows that the most challenging issues are materials properties and model extrapolations to high burnup values. The ceramic nuclear fuel rods operate at high temperatures (~1500 K), and under strong temperature gradients (the order of 4×10^5 Km^{-1}). The basic transport phenomena governing the fuel behavior are the diffusion of chemical species and heat transport. The diffusion is characterized by the diffusivity and the transport of heat by the thermal diffusivity. These two important fuel parameters are related in a complex manner and depend on temperature and fuel composition (non-stoichiometry, for instance). To predict the evolution of fuel performance, these dependencies must be accurately known. In this study we demonstrate that coupling heat and mass transport with changes in stoichiometry is also important for an accurate simulation of fuel behavior. This is a complex computational task that involves a detailed knowledge of UO_2 thermochemistry [3,4].

* Corresponding author.
E-mail address: jcramirez@lanl.gov (J.C. Ramirez).

0022-3115/$ - see front matter
doi:10.1016/j.jnucmat.2006.08.018

Some researchers have performed stress–strain analysis of fuel rods, coupled with heat transfer, e.g. [5,6], but these simulations neglect the effect of non-stoichiometry. This effect can be significant, for example the dependence of thermal conductivity and other thermodynamic properties on non-stoichiometry for mixed oxide fuels and urania can be quite strong [7,8]. Recent simulations of heat transport coupled with oxygen diffusion in CANDU fuel elements [9,10] show that the radial changes in temperature and stoichiometry are strongly coupled. Furthermore, other studies [11] show that in hyper-stoichiometric urania, the heat of transport of oxygen is negative and these ions tend to accumulate in the regions of high temperature due to the so-called thermal diffusion, or Soret effect (the transport of oxygen atoms due to a temperature gradient). Given the strong temperature gradients experienced by nuclear fuel pellets, it is reasonable to expect that thermal diffusion will play a significant role [12–14]. Three-dimensional simulations [15] emphasize the importance of axial heat transport in regions of macroscopic defects, mostly when the fuel pellets are not perfectly cylindrical. However, these simulations have been performed on idealized UO_2 pellets and ignored changes in stoichiometry. The purpose of this work is to evaluate the effect of changes in stoichiometry on the coupled heat and oxygen transport in a fuel element.

2. Models of materials properties

Material properties depend on numerous factors such as temperature, composition, pressure, and atmosphere. In a nuclear reactor, irradiation induces microstructural changes and material properties evolve with time. In this work, we made use of existing theoretical and experimental data and developed simple models that capture the influence of the most critical parameters. The models are summarized in Table 1. Since the focus of the simulations is on transport phenomena in urania, the properties of the cladding and the He gas have been approximated using data from literature [16]. The rate of heat generation due to the fission reactions was also retrieved from literature [17,5]. The specific heat of UO_2 was calculated using experimental data evaluated in SGTE and JANAF tables. The two databases are in good agreement and, for the temperature domain of interest for this work (600–1600 K), a linear interpolation gives:

$$C_p(T) = 264\,256 + 47 \cdot T, \tag{1}$$

where C_p is given in J kg^{-1} K^{-1}. By using Eq. (1) for heat capacity we are neglecting the effect of non-stoichiometry on C_p.

To describe the temperature dependence of UO_2 density, a piecewise function was necessary to distinguish between low and high temperature domains

Table 1
Summary of materials properties (temperature in K)

Property	Dependence on temperature T (K) and stoichiometry x	Units	Source
ρ (UO_2)	$10\,960 \cdot (a + bT + cT^2 + dT^3)^{-3}$	kg m^{-3}	[18]
	$a = 0.997, b = 9.082 \times 10^{-6}$; $c = -2.705 \times 10^{-10}, d = 4.391 \times 10^{-13}$ } $T < 923$ K		
	$a = 0.997, b = 1.179 \times 10^{-5}$; $c = -2.429 \times 10^{-9}, d = 1.219 \times 10^{-12}$ } $T > 923$ K		
k (UO_2)	$k(T,x) = \lambda_0(T) \cdot \frac{\arctan[\theta(T,x)]}{\theta(T,x)} + 5.95 \times 10^{-11} \cdot T^3$ $\lambda_0(T) = [3.24 \times 10^{-2} + 2.51 \times 10^{-4} \cdot T]^{-1}$ $\theta(T,x) = 3.67 \cdot \exp(-4.73 \times 10^{-4} \cdot T) \cdot \sqrt{2 \cdot x \cdot \lambda_0(T)}$	W m^{-1} K^{-1}	[35]
Q^* (UO_2)	$Q*(x) = -1380.8 - 134435.5 \exp(-x/0.0261)$	J mol^{-1}	[13]
F (UO_2)	$F(T,x) = \frac{2+x}{2\cdot(1-3x)\cdot(1-2x)}$		[42]
ρ (He)	$0.0818 - 8.275 \times 10^{-5}\,(T - 600)$	kg m^{-3}	[16]
C_p (He)	5190	J kg^{-1} K^{-1}	
k (He)	$0.0468 + 3.81 \times 10^{-4} T - 6.79 \times 10^{-8} T^2$	W m^{-1} K^{-1}	
ρ (clad)	7817	kg m^{-3}	
Cp (clad)	420	J kg^{-1} K^{-1}	
k (clad)	$10.98 + 0.014\,T - 7.44\,T^2$	W m^{-1} K^{-1}	

[18]. The function is described in Table 1. The expression for density shown in Table 1 is derived in Ref. [18] from data for stoichiometric urania. Nevertheless, the work of Martin [19] suggests that there is little difference for this property between stoichiometric and hyper-stoichiometric fuel. Two other properties of non-stoichiometric urania require more complex models and are discussed below.

2.1. Thermal conductivity of UO_2

The thermal conductivity of UO_2 was extensively studied using experimental methods [20,21] and several recommendations for thermal conductivity have been issued [18,22–24]. The methods are based on laser flash measurements of thermal diffusivity combined with measurements of density and specific heat. The experimental studies show that thermal conductivity of UO_2 decreases with temperature and is strongly influenced by microstructure and defects, especially porosity [25]. Recent studies show that burnup plays a major role in UO_2 transport properties and there are significant differences between thermal conductivity at low and high burnup [26].

Thermal properties of UO_2 have been also investigated using atomistic models based on various inter-atomic potentials. In particular, thermal conductivity was calculated using either equilibrium [27–30], or non-equilibrium [31] molecular dynamics (MD) simulations in a large interval of temperature, from 300 to 2000 K. In these techniques, thermal conductivity is often calculated using the Green–Kubo statistical method.

The conclusion of the atomistic studies is that the main contributions to heat conduction in UO_2 are due to lattice vibrations and electrons. The contribution of point defects, such as oxygen vacancies, interstitials, and small polarons originating from conduction electrons [18], was also included [27]. The experimental observation that thermal conductivity of UO_2 decreases with temperature (up to 2000 K) was confirmed by the MD calculations and attributed to the phonon–phonon interactions. Due to the large atomic weight of UO_2, isotopic effects can be safely neglected, but the influence of grain boundaries and porosity [32–34] is important. That makes the thermal conductivity of polycrystalline samples lower than that of single crystals.

In this work we used the model developed by Amaya et al. [35]. This model is consistent with experimental data of thermal conductivity in UO_{2+x} over a wide range of temperature (300–1400 K) and stoichiometry ($x < 0.2$). All model parameters are given in Table 1.

2.2. Oxygen diffusivity in UO_2

Studies of the mobility of electrons and holes [36,37] as well as diffusion of defects in UO_2 using measurements of electric properties in controlled atmosphere [38] have been performed in isothermal conditions. Although new thermochemical models of defects and oxygen mobility have been recently developed for PuO_{2-x} [39], a comprehensive model of defect formation and oxygen diffusion in UO_{2+x} is still lacking. The evaluation of oxygen diffusivity in UO_{2+x} [40] shows that several mechanisms contribute to oxygen diffusion and the chemical diffusion coefficient decreases with non-stoichiometry, x.

For the purpose of this work, a model that captures the main properties of oxygen diffusivity over a large temperature and stoichiometry interval is desirable. Using a set of experimental values from [40], we have optimized the parameters of the following function describing the chemical diffusivity $D(T,x)$ of oxygen in hyper-stoichiometric urania:

$$\log\left[D(T,x)\right] = -9.386 - \frac{4.26\times 10^3}{T} + 1.2\times 10^{-3} \cdot T\cdot x + 7.5\times 10^{-4}\cdot T\cdot \log\left(\frac{2+x}{x}\right), \tag{2}$$

where $D(T,x)$ is in $m^2\ s^{-1}$ and temperature T is measured in K.

This rather simple expression provides values in good agreement with experiments in the temperature interval (300–1800 K) and for non-stoichiometries $0 < x < 0.2$. It is also consistent with the recent model [40], especially in the low non-stoichiometry regime, $x < 0.03$.

As the models of thermo-mechanical properties of fuel materials evolve and become more accurate, we will include them in the simulation capability.

3. Heat and oxygen diffusion simulation

The simulation domain consisted of a cylindrical UO_2 fuel pellet placed in a steel cladding. The gap between the cladding and the fuel pellet is filled with helium. Fig. 1 shows a 22.5° angular sector of the cylindrical computational domain. The geometry

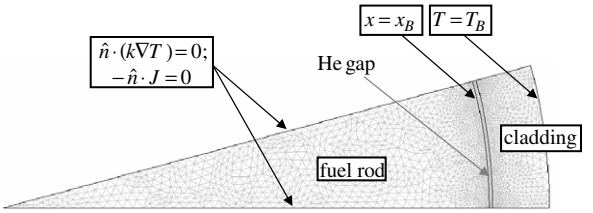

Fig. 1. Representative 'slice' for purely radial simulations showing the main components of the assembly: fuel rod, helium gap and steel cladding. Additionally, we show the analytical expressions representing the boundary conditions. Here, $\hat{n}$ is a unit vector normal to the boundary pointing outwards, T is the temperature, k is the thermal conductivity and J is the oxygen atom flux.

and the mesh have been generated with COMSOL Multiphysics™. The domain shown in Fig. 1 is azimuthally symmetric; hence all simulations are essentially one-dimensional in space (all gradient occur in the radial direction only). Nevertheless, we adopt the two-dimensional domain shown for clarity, and to use this model with little modification in further studies which will include multiple-dimensional effects. For all simulations in this paper, the pellet radius is 4.3 mm, the helium gap width is 0.03 mm, and the cladding width (outer radius minus inner radius) is 0.5 mm. Assuming fission reactions that generate heat at a uniformly distributed constant rate, the heat transfer equation in the fuel pellet is

$$\rho C_p \frac{\partial T}{\partial t} = \nabla \cdot (k \nabla T) + \dot{Q}, \tag{3}$$

where ρ, C_p and k are the density, specific heat at constant pressure, and thermal conductivity, respectively, and t is time.

Since UO_{2+x} is non-stoichiometric, and the model used for thermal conductivity includes a dependence on x, Eq. (3) must be coupled with an equation for oxygen diffusion in the hyper-stoichiometric case [41,13]

$$J = -\frac{1}{2} \cdot n \cdot D(T,x) \cdot \left[\nabla x + \frac{x}{F(T,x)} \frac{Q^*}{RT^2} \nabla T \right], \tag{4}$$

where n is the concentration of regular oxygen sites in UO_2, $F(T,x)$ is the thermodynamic factor of oxygen, Q^* is the heat of transport of oxygen, and R is the universal gas constant. The expression for Q^* we used in this study is listed in Table 1 and comes from a fit of the experimental data reported by Sari and Schumacher [13]. We should point out that despite the fact that the data of reference [13] is for mixed oxides, Fig. 1 in that paper shows only a weak dependence of Q^* on plutonium content, hence our expression for Q^* listed in Table 1 is appropriate for UO_{2+x}. The thermodynamic factor is given by:

$$F(T,x) = 1 + \frac{\partial \ln \gamma_O}{\partial \ln X_O} = \frac{\partial \ln P_O}{\partial \ln X_O} = \frac{1}{2} \cdot \frac{\partial \ln P_{O_2}}{\partial \ln X_{O_2}}, \tag{5}$$

where γ is the activity coefficient of oxygen, and P_O is the partial pressure of oxygen in UO_{2+x}, and X_O is the oxygen concentration. In this work, an analytical expression of $F(T,x)$ was derived using a model of oxygen partial pressure from literature [42] and listed in Table 1.

The oxygen flux J satisfies the equation of continuity expressing the oxygen atoms conservation:

$$\frac{1}{2} \cdot n \cdot \frac{\partial x}{\partial t} = -\nabla \cdot J. \tag{6}$$

In the parenthesis of Eq. (4), the gradient of non-stoichiometry is associated with the conventional Fickian diffusion. The term involving a gradient in temperature represents the Soret effect [43,44], and it is a cross-transport effect: a flux of oxygen appears under a temperature gradient.

The counterbalancing effects of the Soret and Fickian fluxes are responsible for a variation of oxygen concentration through the fuel pellet even under steady-state conditions. Due to the Soret effect, the gradients in temperature experienced by the fuel rod cause a current of oxygen atoms to flow through the pellet, which in turn triggers the conventional Fickian diffusion. Conversely, the temperature variation with position through the pellet in a steady-state is preserved because of the heat generation, which manifests itself as a source term in the heat equation. Sari and Schumacher [13] observed this phenomenon of oxygen redistribution, but did not perform a quantitative evaluation of the change in stoichiometry.

For all simulations reported here, we solve for temperature within the fuel, gap and cladding, and for non-stoichiometry within the fuel pellet only. We use symmetry boundary conditions for T and J along the straight edges of the pellet-cladding assembly (see Fig. 1). We assume perfect thermal contact between the pellet outer surface and the helium gap, as well as between the gap and the steel cladding inner surface. We use a Dirichlet type (fixed value) boundary condition for the temperature at the cladding outer surface, as well as for the non-stoichiometry at the pellet outer surface.

In some cases, as detailed in the following section, these boundary conditions are time-dependent. In Fig. 1 we indicate the analytical expressions describing these boundary conditions.

We consider both steady-state and transient simulations. When solving for steady-states, we set the temperature everywhere in the pellet equal to the imposed temperature at the outer surface of the cladding, and the non-stoichiometry in the pellet equal to the value imposed at the outer surface of the pellet, as initial conditions. In all cases, we exercise care, so that results are independent of the mesh size distribution.

To solve the heat and species equation, we employ quadratic Lagrange elements and a nonlinear iterative technique with a nested linear solver. Within COMSOL Multiphysics™, we chose the default un-symmetric multi-frontal method (UMFPACK) as a linear solver.

4. Results and discussion

4.1. One-dimensional, steady-state simulations

We consider the case where all heat conduction and oxygen diffusion takes place along the radial direction only, at steady-state. According to Eqs. (3) and (6), in this case the time derivatives are zero. Therefore, the local non-stoichiometry does not explicitly depend on time, which implies that under steady-state conditions, the number of oxygen atoms within a fuel rod remains constant, a condition which is only fulfilled with $J = 0$, so Eq. (4) ensures that the flux of oxygen atoms vanishes (i.e., J is 0 everywhere in the pellet, even including $r = 0$). Since $J = 0$, the oxygen diffusivity plays no role in the steady-state solution. We program the steady-state versions of Eqs. (3) and (6) into COMSOL Multiphysics™ in the domain shown in Fig. 1, which is a cross section normal to the cylindrical axis of the fuel pellet-steel cladding arrangement. By enforcing the symmetry (zero flux) boundary conditions along the straight edges, we are ensuring only radial flow of oxygen and heat. For the temperature at the outer face of the steel cladding we set a Dirichlet type boundary condition specifying the temperature there at 750 K, which represents a typical operating temperature. For the outer edge of the fuel rod, we set a representative value of the non-stoichiometry of 0.02. For the heat generation rate due to the fission reaction, we use 2×10^8 W m^{-3} which, given the dimensions of the fuel pellet, is equivalent to a linear power level of approximately 11 kW m^{-1}.

Fig. 2 shows the temperature (solid line) and non-stoichiometry (dashed line) distributions along the radial direction of a fuel rod. Since heat is extracted at the outer surface of the cladding, the temperature decreases with increasing radius, as expected. Since the heat of transport of oxygen Q^* in hyper-stoichiometric urania is negative, the oxygen atoms re-distribute through the pellet such that there is a higher hyper-stoichiometry in the hotter regions. Fig. 3 presents the effects of the x-dependent terms in the thermal conductivity. We compare the profiles obtained when using the expression for $k(x, T)$ from Table 1 with respect to those obtained

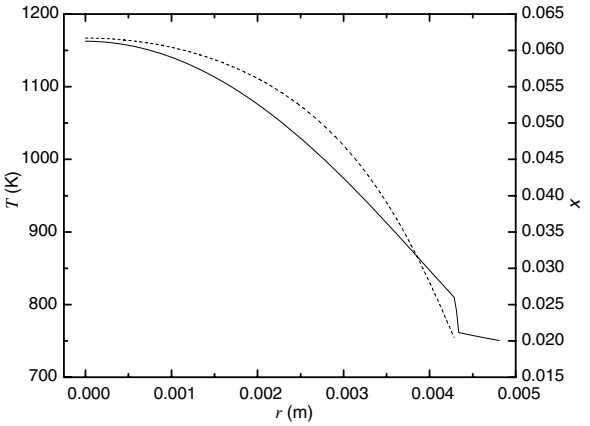

Fig. 2. Steady-state temperature (solid line) and non-stoichiometry (dashed line) distribution in radial direction for a UO_2 fuel rod.

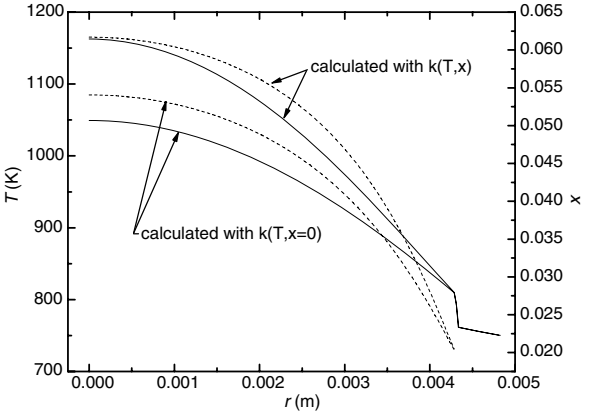

Fig. 3. Comparison of steady-state temperature and non-stoichiometry profiles calculated with and without x dependence on the expression for thermal conductivity of the fuel.

by omitting the effect of non-stoichiometry in the thermal conductivity. To obtain an x-independent expression for k, we set $x = 0$ in the expression for $k(x,T)$ of Table 1. The expression $\text{atan}(\theta)/\theta \to 0$ as $x \to 0$, so we used this limiting value. From the expression for $k(x,T)$ from Table 1, the thermal conductivity decreases with increasing non-stoichiometry. For the same heat flux, according to Fourier's law, a lower thermal conductivity implies a higher temperature gradient. Since the wall temperature is the same, the case where we corrected the conductivity for non-stoichiometry should present a higher core temperature, as is shown in Fig. 3. We observe that not including the x-dependence on thermal conductivity in causes an underestimation of the temperature of almost 100 K for the conditions considered in this particular case. This 100 K difference, however, can be greatly affected by the heat generation rate intensity and the boundary conditions. Fig. 3 also shows that the non-stoichiometry near the rod center is underestimated when the thermal conductivity is not corrected for x-dependency.

The heat generation rate can vary widely depending on reactor operating conditions. Fig. 4 shows the temperature at the pellet center, $T_{\max}$, as a function of the non-stoichiometry at the outer face of the fuel pellet, x_B, for several values of $\dot{Q}$. We consider the values of the heat generation rate ranging from 10^7 W m^{-3} to 3×10^8 W m^{-3}. With a fuel pellet radius of 4.3 mm, these heat generation rates correspond to linear power levels of 0.6 kW m^{-1}, to 17.4 kW m^{-1}, respectively. Each data point in this figure is the result of one steady-state simulation. When the heat generation rate is higher, a small variation in the non-stoichiometry at the rod outer surface has a more marked effect on the maximum temperature within the rod. An important conclusion from Fig. 4 is the fact that strongly non-stoichiometric rods will experience very high temperatures. Additionally, since the oxygen atoms tend to be redistributed towards the hotter regions, the increase in temperature with $\dot{Q}$ is accompanied by an increase in x. The value of x at the outer face of the rod is related to the initial non-stoichiometry of the pellet and to the oxygen removal rate towards the helium-filled gap. It is expected that the higher the deviation from stoichiometry, the higher the temperature at the center of the rod. This is related to the effect of x on the thermal conductivity: higher values of x cause lower values of k, which in turn cause higher temperatures within the rod.

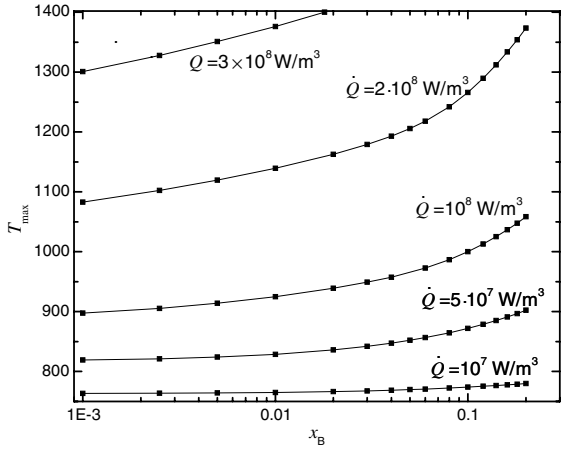

Fig. 4. Steady-state temperature at the center of the rod, $T_{\max}$, for different heat generation rates $\dot{Q}$ in W/m^3, as a function of the non-stoichiometry at the outer surface of the fuel rod, x_B. In all cases shown, the temperature at the outer face of the steel cladding is kept at 750 K. Each point in the plot is the result of a steady-state calculation and the lines between data points are meant only as a guide to the eye.

4.2. One-dimensional, transient simulations

The diffusion of heat and of chemical species, generally occur over quite different time scales. The characteristic time for heat diffusion is given by L^2/α, where L is the length scale of the problem and $\alpha = k/(\rho\, C_p)$ is the thermal diffusivity. The characteristic time for diffusion of species is given by L^2/D. Under certain conditions, these characteristic times can be vastly different. We can gain considerable insight with simple order-of-magnitude calculations. Taking $x = 0.01$ and $T = 1000$ K, Eq. (2) yields $D = 2.0\times10^{-14}$ m^2 s^{-1}. At the same values of x and T, the thermal diffusivity is $\alpha = 8.3\times10^{-10}$ m^2 s^{-1}. Setting $L = 4.3\times10^{-3}$ m, the pellet radius, we calculate the characteristic times to be 1.9×10^4 s (≅5.3 h) for heat, and 1.5×10^7 s (≅172 days) for oxygen diffusion. The ratio of the species to heat diffusion times is known as the Lewis number, $Le = \alpha/D$ and can be interpreted as ratio of the time required by the x field to reach a steady-state, to the time required for the T field to reach a steady-state.

With the correlations for density, conductivity, specific heat and oxygen diffusivity, we can calculate the Lewis number. Fig. 5 shows a plot of Le as a function of x for selected values of the temperature. Note that Le can be as high as almost 10^5. The char-

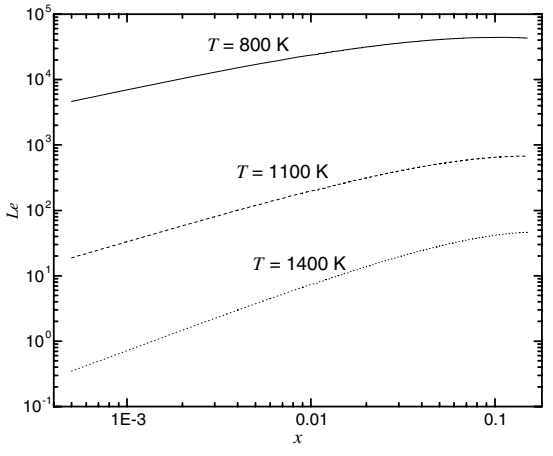

Fig. 5. Plot of the Lewis number ($Le = \alpha/D$), where α is the thermal diffusivity as a function of non-stoichiometry, for selected values of temperature. The Lewis number represents the ratio of characteristic times for species diffusion time to that of heat diffusion. For strongly non-stoichiometric fuel pellets at low temperatures, *Le* can be up to almost 10^5, which implies that changes in the temperature distribution can occur with negligible changes in the non-stoichiometry distribution.

acteristic times of heat and oxygen diffusion are useful in estimating how long the reactor will take to adjust to a change in operating conditions, or to determine how long the reactor will take to achieve a steady-state after initial startup. Fig. 5 shows that for $x > 0.05$, the Lewis number becomes practically independent of x, especially at low temperatures. For strongly non-stoichiometric fuel pellets at low temperatures, *Le* can be up to almost 10^5, which implies that changes in the temperature distribution can occur with negligible changes in the non-stoichiometry distribution. Conversely, for almost stoichiometric pellets ($x < 0.001$) at sufficiently high temperatures, *Le* can be smaller than 1, thus indicating that oxygen atoms diffuse faster than heat. This disparity in the characteristic diffusion times plays an important role in the transient behavior of the fuel under sudden changes in the operating conditions. We examine in more detail this transient behavior in the following.

4.2.1. Start-up of reactors

We examine the transient behavior of the temperature and non-stoichiometry distributions when the reactor is started from ambient conditions. We assume that the pellet possesses a spatially uniform x distribution, $x = x_0$ and the temperature is $T_0 = 750$ K everywhere. At time $t = 0$, the heat generation rate starts to vary from an initial value $\dot{Q}_0 = 0$ W m^{-3}, and quickly (within 10 min) reaches a value of $\dot{Q}_{\max} = 2 \times 10^8$ W m^{-3}, according to

$$\dot{Q}(t) = \dot{Q}_0 + \frac{\dot{Q}_{\max} - \dot{Q}_0}{1 + 10 \cdot \exp\left[-(-10 + t/\tau)\right]}, \tag{7}$$

where $\tau = 45$ s is a time constant. We should point out that Eq. (7) is not an attempt to accurately model the dynamics of the nuclear reaction, but must be interpreted simply as an *ad-hoc* model of a quickly varying power source, convenient for the purposes of this study.

We examined three cases: weak, moderate, and strong non-stoichiometry corresponding to $x_0 =$ 0.001, 0.01, and 0.1, respectively, and the results are shown in Fig. 6. The solid lines are the ratio of the temperature at the center of the pellet, $T_{\max}$ to the initial uniform temperature T_0. A quasi-steady temperature is reached and maintained after $t \sim 5 \times 10^4$ s (14 h), regardless of the value of x_0. Although there are some temperature variations beyond this point, these are insignificant. The ratio x/x_0 at the center is shown in dashed lines. Note that the weaker the non-stoichiometry, the largest the variation in the non-stoichiometry profile with respect to the initial condition. For instance, the weakly non-stoichiometric pellet ($x_0 = 0.001$) attains a value of x at the pellet center almost 30

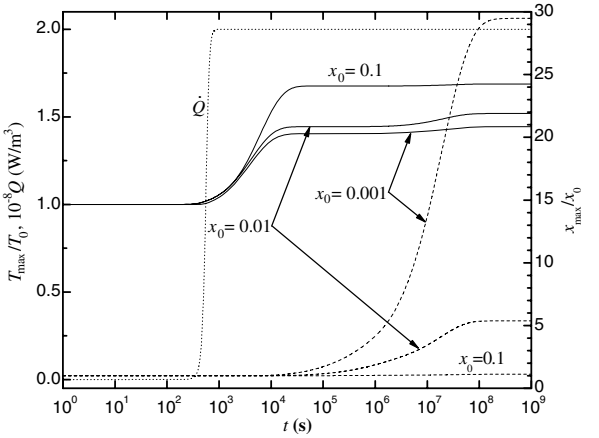

Fig. 6. Transient response for start-up of reactor from ambient conditions. The initial condition is a uniform non-stoichiometry, x_0, and a uniform temperature T_0. The heat generation rate is increased from 0 to 2×10^8 W/m^3 in the course of approximately 10 min, as shown by the dotted line, while keeping the outer face of the fuel pellet at x_0 and the outer face of the cladding at $T_0 = 750$ K. We show results for three values of x_0. The presence of a quasi-steady-state for the temperature after after $t \sim 5 \times 10^4$ s while x is still varying is a consequence of the large values of the Lewis number.

times larger than x_0. On the other hand, the strongly non-stoichiometric pellet sees an increase of only 11% (almost non-appreciable in Fig. 6) in the non-stoichiometry at $r = 0$. These changes in the non-stoichiometry at the center become significant after about $t \sim 10^7$ s, or about 115 days. The non-stoichiometry distribution does not reach a true steady-state until $t \sim 10^8$ s, or a little over 3 years. This is expected given our previous discussion on the Lewis number and its physical significance. With these extremely long characteristic times for oxygen diffusion it is not uncommon to neglect the effects of oxygen redistribution on the temperature profile.

4.2.2. Time-dependent heat generation rate

We consider now the behavior of the pellet when subjected to a change in the heat generation rate intensity. As initial condition, we use the x and T distributions obtained from a steady-state simulation in which the steel cladding had a surface temperature of 750 K and the outer face of the fuel rod has a non-stoichiometry of 0.001. The simulation started with the steady-state situation and the heat generation rate is $\dot{Q} = 10^7\ \mathrm{W\,m^{-3}}$. Then $\dot{Q}$ was increased up to $2 \times 10^8\ \mathrm{W\,m^{-3}}$over the course of about 10 min according to Eq. (7), with $\dot{Q}_0 = 10^7\ \mathrm{W\,m^{-3}}$ as the heat generation rate at the beginning of the transition, $\dot{Q}_{\max} = 2 \times 10^8\ \mathrm{W\,m^{-3}}$ as the new heat generation rate and $\tau = 45$ s. Fig. 7 shows that this change corresponds to going along the $x = 0.001$ vertical from the $\dot{Q} = 10^7\ \mathrm{W\,m^{-3}}$ curve to the $\dot{Q} = 2 \times 10^8\ \mathrm{W\,m^{-3}}$ curve.

Fig. 7 shows the externally imposed variation of the heat generation rate (dotted line), i.e., Eq. (7), which occurs in about 10 min. The solid and dashed lines show variation of the temperature at the center, $T_{\max}$ and the non-stoichiometry at the center, $x_{\max}$. We see that the temperature adopts a new quasi-steady value of around 1050 K after the change in heat generation rate. The small lag between the change in $\dot{Q}$ and the new temperature plateau of about 1050 K is due to the finiteness of the heat diffusion characteristic time. It is slightly after $t = 10^5$ s that a change in $x_{\max}$ becomes noticeable, long after the temperature has reached its 1050 K plateau, with the steady value of $x_{\max}$ reached only after $t = 10^8$ s. This severe time lag between heat and species diffusion is the effect of the Lewis number. The significant changes in the non-stoichiometry profile after about $t = 10^7$ s affects the material properties, and this explains the adjustment of the temperature at a new plateau close to 1060 K. Again, because of the magnitude of the Lewis number, the temperature 'adapts' to changes in non-stoichiometry almost instantly. Fig. 7 shows that changing $\dot{Q}$, a parameter which is heavily influential on the temperature profile, creates two transient regimes: an 'early' regime during which the temperature profile quickly adapts to the new value, but the non-stoichiometry distribution has not 'felt' the change yet, and a 'late' regime where the x profile adjusts to the new conditions and this adjustment is accompanied by instantaneous changes in the temperature profile.

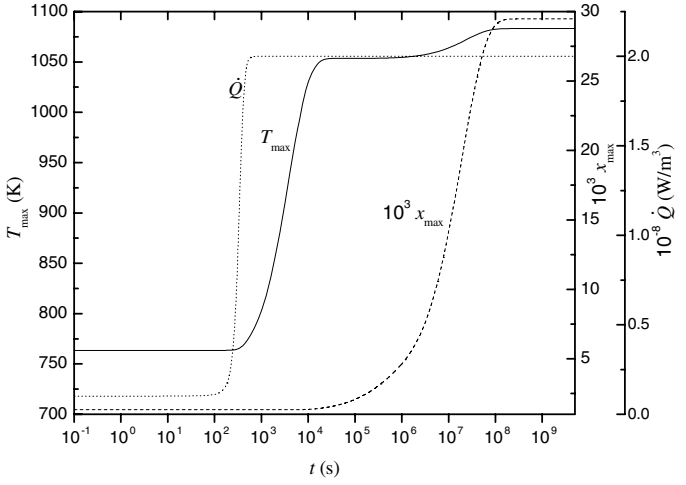

Fig. 7. Transient response to an increase in the heat generation rate $\dot{Q}$ from $10^7\ \mathrm{W/m^3}$ to $2 \times 10^8\ \mathrm{W/m^3}$, while maintaining the outer surface of the cladding at 750 K and the pellet outer surface non-stoichiometry at 10^{-3}. The plot shows the temperature (solid line) and the non-stoichiometry at the pellet center (dashed line) as well as the heat generation rate (dotted line).

As discussed in connection with Eq. (4), the flux of oxygen atoms is comprised of two currents, and hence there are two driving forces for oxygen diffusion. The driving force j_F, associated with Fickian diffusion is the non-stoichiometry gradient, ∇x, while the driving force j_S, for Soret diffusion is the second term in the parenthesis of Eq. (4). Fig. 8 shows the temporal variation of j_F (dashed line) and j_S (solid line) for the same conditions of Fig. 7, as well as their sum, $j_F + j_S$ (dotted line). All the quantities shown in Fig. 8 are evaluated at the pellet outer surface. Note that at early and late times ($t < 10^2$ s; $t > 10^8$ s) when the system is at steady-states, j_F and j_S are of equal magnitude but of opposite signs, hence their sum is zero, as was discussed in connection with the steady-state simulations. Given the profiles of Figs. 2 and 3, it is expected to observe negative gradients of non-stoichiometry (or negative values of j_F), so the fact that during ($\sim 10^4$ s$> t > \sim 5 \times 10^6$ s) we observe positive values of j_F deserves further attention. Fig. 9 shows the x profiles at selected times during the change of heat generation rate. The profiles for $t = 10^5$ s and $t = 10^6$ s show profiles with a positive x gradient near the pellet outer surface. Therefore, at these instants and at near the pellet outer surface, both the Soret and Fickian fluxes are directed towards the inside of the pellet.

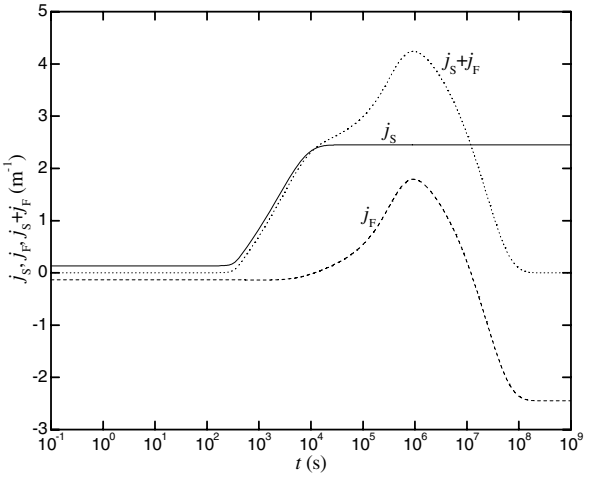

Fig. 8. Transient variation of the driving forces for Soret (solid) and Fickian (dashed) fluxes between two steady-states at $r = 4.3 \times 10^{-3}$ m, during an imposed increase in the heat generation rate, $\dot{Q}$ from 10^7 W/m^3 to 2×10^8 W/m^3. We maintained the outer surface of the cladding at 750 K and the pellet outer surface non-stoichiometry at 10^{-3}. The dashed line represents the sum of both driving forces. The driving forces are equal and of opposite signs at the steady-states corresponding to the beginning and end conditions.

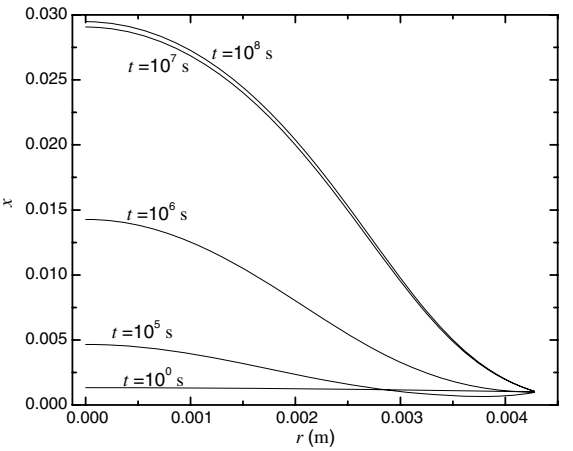

Fig. 9. Profiles of non-stoichiometry at selected times during the change of heat generation rate, $\dot{Q}$ from 10^7 W/m^3 to 2×10^8 W/m^3. We maintained the outer surface of the cladding at 750 K and the pellet outer surface non-stoichiometry at 10^{-3}. At some times during transient behavior (e.g., $t = 10^5$ s and 10^6 s), we observe a positive x gradient near the surface of the pellet.

This simulation proves that a change in the heat generation rate, a crucial parameter determining the temperature profile, affects rather quickly the temperature distribution which in turn affects the non-stoichiometry profile after longer periods of time. We observed interesting dynamics between the Soret and Fickian atom fluxes when passing from one steady-state to another, noting that these effects produce oxygen atom currents that do not cancel each other as in the steady-state.

4.2.3. Time-dependent non-stoichiometry boundary condition

This simulation shows the transient response of the fuel element to a sudden change in the non-stoichiometry at the outer face of the fuel pellet. This corresponds to a change in the rate at which the oxygen is being extracted within the helium-filled gap. We considered the transition between two steady-states. In the first steady-state, the non-stoichiometry at the outer face is $x_B = 0.001$ and over the course of approximately 10 min, we change x_B to 0.2, while keeping the temperature at the outer face of the steel cladding at 750 K and the heat generation rate at $\dot{Q} = 2 \times 10^8$ W m^{-3}. According to Fig. 4, this corresponds to moving from the $x = 0.001$ to the $x = 0.2$ points along the $\dot{Q} = 2 \times 10^8$ W m^{-3} curve. The form of the boundary condi-

tion for x was similar to the change in heat generation rate in Section 4.2.1:

$$x_B(t) = x_{B_0} + \frac{x_{B,\max} - x_{B,0}}{1 + 100 \cdot \exp\left[-(-5 + t/\tau)\right]}, \quad (8)$$

where $x_B(t)$ is the time-dependent non-stoichiometry at the boundary (the outer face of the fuel rod), and $x_{B,0}$ and $x_{B,\max}$ are the initial and final values, respectively, of the non-stoichiometry at the boundary. From Eq. (8), the transition from $x_{B,0}$ to $x_{B,\max}$ occurs over approximately 10 min. Fig. 10 shows the transient response to the increase in the non-stoichiometry at the outer face given by Eq. (8). As expected, the non-stoichiometry at the center of the pellet, $x_{\max}$ reacts slowly to the change in the boundary condition, reflecting the large time scales associated with oxygen diffusion. The changes in the x profile introduced by the time-varying boundary condition for x_B affect the material properties. This explains the rather weak change in the temperature at the center as soon as the new steady value of x_B is achieved. The significant changes in the center temperature occur after very long times have elapsed and these changes are an instant response to the change in the x profile. Note the significant time lag between the achievement of a steady value for x_B and reaching a time-independent value for $x_{\max}$.

In this section, we used a time-dependent boundary condition for x. Unlike for a change in the heat generation rate, we do not observe an 'early' regime during which the temperature experiences vast changes rather independently of x, but rather all changes occur at a time scale dictated by the diffusion of oxygen atoms.

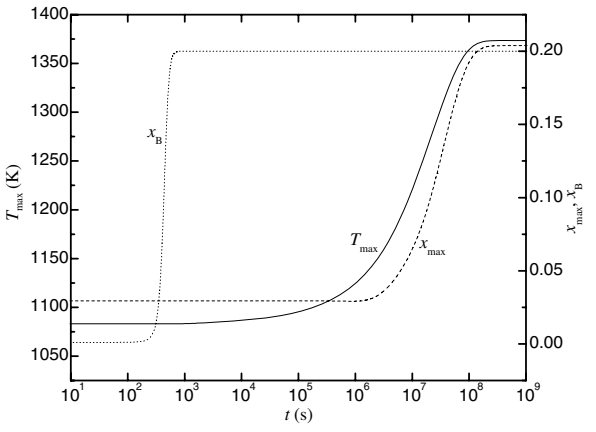

Fig. 10. Transient response to an increase in the non-stoichiometry at the outer face of the fuel pellet, x_B from 0.001 to 0.2, for $\dot{Q} = 2 \times 10^8$ W/m^3, and a fixed temperature of 750 K at the outer surface of the cladding. The dashed line is the non-stoichiometry at the center of the pellet, $x_{\max}$ and the solid line is the temperature at the center of the pellet, $T_{\max}$. The dotted line is the externally imposed boundary condition of Eq. (8).

5. Conclusions

We solve the one-dimensional heat and oxygen atom diffusion problem for a UO_{2+x} fuel rod, under steady-state and time-dependent situations. We solved for the non-stoichiometry distribution in the fuel rod and for the temperature distribution in the steel cladding and the fuel rod, as well as in the gap that separates them. The mathematical model is a set of highly coupled, non-linear partial differential equations for which we used the commercial finite-element package COMSOL Multiphysics™. We employed expressions for thermal conductivity, k and chemical diffusivity, D reflecting a dependence of these properties on temperature and non-stoichiometry. The expressions for k and D came from previously published correlations, or from analyses of published data.

In steady-state simulations, we observed that the influence of x on the thermal conductivity can lead to significant corrections of the maximum temperature on the fuel rod. In steady-state, for a pore-free sample, the temperature and non-stoichiometry profiles exhibit negative gradients in the radial direction (both decrease with increasing r). This is due to the fact that, in steady-state, the Soret (atoms diffusing towards region of higher temperature) and Fickian (atoms diffusing towards region of lower non-stoichiometry) oxygen currents counter-balance each other. From parametric studies, we observe that strongly non-stoichiometric rods of UO_{2+x} will experience higher core temperatures than weakly non-stoichiometric rods, for the same heat generation rate, and that an increase in the heat generation rate causes a higher core temperature in a strongly non-stoichiometric rod than that caused in a weakly non-stoichiometric rod.

We performed transient simulations by introducing a time-dependent heat generation rate, or boundary condition for x between two steady-states. When changing the heat generation rate, a 'thermal' parameter, we observed the temperature profile rapidly adjusting to the new conditions in an 'early' regime, while the x profile exhibits a significant lag, adjusting over a much extend time period, or 'late' regime. Small variations of the T

profile in the 'late' regime reflect the change in thermal properties exerted by the change in the x profile. When changing the boundary condition for the non-stoichiometry, we observed the characteristic time scale for oxygen diffusion to be the limiting factor for both T and x profile changes. During transient behavior, the Soret and Fickian oxygen atom fluxes do not counter-balance and in some instances act in the same direction.

For future directions, we are considering ways to incorporate the effects of porosity and three-dimensionality on our simulations.

References

[1] P.R. Vasudeva Rao, S. Anthonysamy, M.V. Krishnaiah, V. Chandramouli, J. Nucl. Mater. 348 (2006) 329.
[2] H.S. Aybar, P. Ortego, Prog. Nucl. Energy 46 (2005) 127.
[3] D.R. Olander, Pure Appl. Chem. 67 (1995) 1003.
[4] A. Nakamura, T. Fujino, J. Nucl. Mater. 149 (1987) 80.
[5] M.A. Feltus, K. Lee, J. Nucl. Mater. 7 (1996) 553.
[6] K. Lassmann, H. Blank, Nucl. Eng. Des. 106 (1988) 291.
[7] Y. Philipponneau, J. Nucl. Mater. 188 (1992) 194.
[8] V.A. Kurepin, J. Nucl. Mater. 303 (2002) 65.
[9] B.J. Lewis, W.T. Thompson, F. Akbari, D.M. Thompson, C. Thurgood, J. Higgs, J. Nucl. Mater. 328 (2004) 180.
[10] B.J. Lewis, B. Szpunar, F.C. Iglesias, J. Nucl. Mater. 306 (2002) 30.
[11] E.A. Aitken, J. Nucl. Mater. 30 (1969) 62.
[12] M.G. Adamson, R.F.A. Carney, J. Nucl. Mater. 54 (1974) 121.
[13] C. Sari, G. Schumacher, J. Nucl. Mater. 61 (1976) 192.
[14] Hj. Matzke, J. Less-Common Metals 121 (1986) 537.
[15] S.D. Yu, S. Xu, Nucl. Eng. Des. 216 (2002) 165.
[16] A. Bejan, Heat Transfer, first ed., John Wiley, New York, 1993.
[17] L. Yun, Y. Yuan, A. Romano, M. Kazimi, Fission gas release models of heterogeneous fuels for plutonium burning, in: Proceedings of the 2004 International Meeting on LWR Fuel Performance, No. 1056, 2004, p. 631.
[18] J.K. Fink, J. Nucl. Mater. 279 (2000) 1.
[19] D.G. Martin, J. Nucl. Mater. 152 (1988) 94.
[20] C.G.S. Pillai, A.M. George, J. Nucl. Mater. 200 (1993) 78.
[21] R.L. Gibby, J. Nucl. Mater. 38 (1971) 163.
[22] C. Ronchi, M. Sheindlin, M. Musella, G.J. Hyland, J. Appl. Phys. 85 (1999) 776.
[23] G.J. Hyland, J. Nucl. Mater. 113 (1983) 125.
[24] D.G. Martin, J. Nucl. Mater. 110 (1982) 73.
[25] P.G. Lucuta, H. Matzke, I.J. Hastings, J. Nucl. Mater. 232 (1996) 166.
[26] C. Ronchi, M. Sheindlin, D. Staicu, M. Kinoshita, J. Nucl. Mater. 327 (2004) 58.
[27] T. Arima, S. Yamasaki, Y. Inagaki, K. Idemitsu, J. Alloys Compd. 400 (2005) 43.
[28] K. Kurosaki, K. Yamada, M. Uno, S. Yamanaka, K. Yamamoto, T. Namekawa, J. Nucl. Mater. 294 (2001) 160.
[29] K. Yamada, K. Kurosaki, M. Uno, S. Yamanaka, J. Alloys Compd. 307 (2000) 10.
[30] J.H. Harding, D.G. Martin, J. Nucl. Mater. 166 (1989) 223.
[31] S. Motoyama, Y. Ichikawa, Y. Hiwatari, A. Oe, Phys. Rev. B, Condens. Mat. (USA) 60 (1999) 292.
[32] S.L. Hayes, K.L. Peddicord, J. Nucl. Mater. 202 (1993) 87.
[33] K. Bakker, H. Kwast, E.H.P. Cordfunke, J. Nucl. Mater. 226 (1995) 128.
[34] K. Bakker, H. Kwast, E.H.P. Cordfunke, J. Nucl. Mater. 223 (1995) 135.
[35] M. Amaya, T. Kubo, Y. Korei, J. Nucl. Sci. Technol. 33 (1996) 636.
[36] N.D. Morelon, D. Ghaleb, J.M. Delaye, L. Van Brutzel, Philos. Mag. 83 (2003) 1533.
[37] J.C. Killeen, J. Nucl. Mater. 92 (1980) 136.
[38] G. Chirlesan, D. Chirlesan, S. Anghel, I. Iorga-Siman, J. Optoelectron. Adv. Mater. 4 (2002) 59.
[39] M. Stan, P. Cristea, J. Nucl. Mater. 344 (2005) 213.
[40] P. Ruello, G. Chirlesan, G. Petot-Ervas, C. Petot, L. Desgranges, J. Nucl. Mater. 325 (2004) 202.
[41] S.R. De Groot, Thermodynamics of irreversible processes, North Holland Publ. Co., Amsterdam, 1951.
[42] T.B. Lindemer, T.M. Besmann, J. Nucl. Mater. 130 (1985) 473.
[43] J. Janek, H. Timm, J. Nucl. Mater. 255 (1998) 116.
[44] C. Korte, J. Janek, H. Timm, Solid State Ionics 101/103 (1997) 465.